The Astrophysical Journal, 862:142 (11pp), 2018 August 1 https://doi.org/10.3847/1538-4357/aacef8

$z \sim 2.5$–3 Ionizers in the GOODS-N Field

L. H. Jones[1], A. J. Barger[1,2,3], L. L. Cowie[3], P. Oesch[4], E. M. Hu[3], A. Songaila[3], and R. P. Naidu[5]
[1] Department of Astronomy, University of Wisconsin-Madison, 475 N. Charter Street, Madison, WI 53706, USA
[2] Department of Physics and Astronomy, University of Hawaii, 2505 Correa Road, Honolulu, HI 96822, USA
[3] Institute for Astronomy, University of Hawaii, 2680 Woodlawn Drive, Honolulu, HI 96822, USA
[4] Geneva Observatory, Université de Genève, Chemin des Maillettes 51, 1290 Versoix, Switzerland
[5] Harvard-Smithsonian Center for Astrophysics, 60 Garden Street, Cambridge, MA 02138, USA
Received 2018 April 12; revised 2018 June 18; accepted 2018 June 21; published 2018 August 1

Abstract

We use deep F275W imaging from the *Hubble* Deep UV Legacy Survey (HDUV) and G280 grism spectroscopy from the *Hubble Space Telescope*/WFC3, along with new and archival optical spectra from Keck/DEIMOS, to search for candidate ionizing sources in the GOODS-N field at $z \sim 2.5$–3. Spectroscopic identification of our UV-selected sources are 99% complete to F275W = 25.5 in the region of the UV imaging, and we identify six potential ionizing galaxies or active galactic nuclei (AGNs) at $z \sim 3$. By far the brightest of these is a $z = 2.583$ AGN that totally dominates the ionizing flux in the region, with a specific ionizing volume emissivity at 912 Å of $\epsilon_{912} = 8.3^{27}_{1.4} \times 10^{24}$ erg s^{-1} Hz^{-1} Mpc^{-3}. Based on our spectroscopic data, we find that four candidates are contaminated by foreground galaxies at $z \sim 0.5$–0.7. At $\epsilon_{912} = 2.2^{7.2}_{0.4} \times 10^{23}$ erg s^{-1} Hz^{-1} Mpc^{-3}, the remaining candidate galaxy's contribution to the ionizing background lies well below the flux required to ionize the intergalactic medium at $z \sim 2.5$–3, consistent with previous observations that show that AGNs provide the bulk of the ionizing background at these redshifts.

Key words: cosmology: observations – galaxies: active – galaxies: distances and redshifts – galaxies: evolution – galaxies: formation

1. Introduction

One of the most pressing issues in modern observational cosmology is the identification of sources that contribute to the metagalactic ionizing background, particularly in the era of cosmic reionization—an important epoch in the history of the universe that saw the formation of the first stars and galaxies at $z \gtrsim 6$ (e.g., Bouwens et al. 2006, 2012, 2015a; Ouchi et al. 2009; Robertson et al. 2015). Star-forming galaxies and active galactic nuclei (AGNs) both contribute to the production of ionizing photons, though their relative importance appears to evolve with cosmic time. Most evidence currently favors a scenario in which low-luminosity star-forming galaxies are the primary drivers of hydrogen reionization (Riccoti & Shull 2000; Bouwens et al. 2006; Fontanot et al. 2007, 2014; Robertson et al. 2010, 2015; Japelj et al. 2017), while AGN contributions to the ionizing background are small until $z \sim 2$–3 (Barger et al. 2003; Bolton et al. 2005; Cowie et al. 2009; Georgakakis et al. 2015; Cristiani et al. 2016; Smith et al. 2018; Puchwein et al. 2018). However, some authors have argued that quasars/AGNs could remain important at very high redshifts, producing a non-negligible or even dominant fraction of UV photons during the era of reionization (e.g., Fontanot et al. 2012; Giallongo et al. 2015; Madau & Haardt 2015).

One motivation for these latter studies is to relax constraints on the escape fraction, $f_{\rm esc}$, needed to produce the observed ionizing background at high redshift; these constraints are imposed by a faint galaxy dominated reionization scenario. Indeed, determining a value for $f_{\rm esc}$, which is the fraction of all Lyman continuum (LyC, rest frame $\lambda < 912$ Å) photons that manage to escape their galaxy of origin to ionize the intergalactic medium (IGM), has been a major focal point of research on reionization. Most theoretical and semianalytical models of reionization require an average $f_{\rm esc}$ of about 10% or greater for star-forming galaxies (e.g., Bolton & Haehnelt 2007; Vanzella et al. 2012; Feng et al. 2016; Price et al. 2016; Kimm et al. 2017; see, however, Faucher-Giguère et al. 2008 and Matthee et al. 2017), though at the highest redshifts $f_{\rm esc}$ remains largely unconstrained by observations. For sources at $z \gtrsim 4$, the low transmissivity of the IGM effectively prohibits direct measurements of $f_{\rm esc}$ (Madau 1995; Songaila 2004; Inoue et al. 2014). Thus, observations focused on analogous objects at slightly lower redshifts are used to constrain the ionization history of the universe.

Previous individual detections or stacked data analyses suggest small values of $f_{\rm esc}$ in the local universe, at most ~1%–3% (e.g., Leitherer et al. 1995; Steidel. et al. 2001; Grimes et al. 2009; Cowie et al. 2010; Leitet et al. 2013; Rutkowski et al. 2016), with some indications that the escape fraction increases with decreasing UV luminosity and/or increasing redshift (e.g., Mitra et al. 2013; Fontanot et al. 2014; Faisst 2016; Khaire et al. 2016; Japelj et al. 2017). Significant object-to-object variance and differences in the average $f_{\rm esc}$ between types of sources (i.e., $f_{\rm esc} \gtrsim 0.5$ for AGNs versus a few percent for galaxies) further complicates the quest for a reliable measurement of the global ionizing escape fraction (Fernandez-Soto et al. 2003; Ma et al. 2015; Cristiani et al. 2016; Grazian et al. 2016; Guaita et al. 2016).

Much effort has thus been expended in building up a statistically significant population of LyC-emitting sources across a range of redshifts. A handful of strong LyC emitters have been detected in the local universe using data from the Sloan Digital Sky Survey, the COS spectrograph on the *Hubble Space Telescope* (*HST*), and other facilities (e.g., Bergvall et al. 2013; Borthakur et al. 2014; Izotov et al. 2016a, 2016b, 2018; Leitherer et al. 2016). Additional individual detections at redshifts ~2–3 have been made, albeit with some contamination from foreground objects (e.g., Vanzella et al. 2010a, 2010b, 2012; Mostardi et al. 2015; Siana et al. 2015; Grazian

et al. 2016; Shapley et al. 2016), while stacking analyses tend to give a relatively weak average LyC signal at $z \gtrsim 3$ (e.g., Rutkowski et al. 2017; Marchi et al. 2018; Naidu et al. 2018; Steidel et al. 2018).

The GOODS-North and South fields (Giavalisco et al. 2004) are particularly attractive targets for LyC-emitter searches due to the abundance of ancillary data, including thorough spectroscopic coverage. For example, Cowie et al. (2009; hereafter CBT09) used a sample of X-ray selected broad-line AGNs in the GOODS-N to estimate the contributions of AGNs and galaxies to the ionizing background over $0 < z < 5$. They found a 2σ upper limit of 0.008 for the escape fraction for galaxies at $z \sim 1.15$ and, interestingly, that the AGN contribution at similar redshifts is dominated by a small number of far-UV (FUV)-bright quasars. Siana et al. (2010) used *HST* imaging of the GOODS fields to search for LyC emission at $z \sim 1.3$ and constrain the relative escape fraction ($f_{\rm esc,rel}$, the LyC flux relative to the UV continuum flux, typically at 1500 Å). They found a stacked upper limit of $f_{\rm esc,rel} < 0.02$ with no galaxies in their sample detected individually. More recently, Grazian et al. (2017) used *U*- and *R*-band imaging from the Large Binocular Telescope to constrain the escape of LyC photons at $z \sim 3.3$ in several deep fields, including the GOODS-N field, and found $f_{\rm esc,rel}$ is at most 1.7% for their stacked image of 69 star-forming galaxies. Meanwhile, a particularly strong LyC candidate at $z \sim 3.2$ in the GOODS-S, known as *Ion2*, was discovered by Vanzella et al. (2015) and later confirmed by Vanzella et al. (2016) and de Barros et al. (2016), who found it to be a compact, low-metallicity source with an absolute escape fraction upwards of 50%.

Naidu et al. (2017) identified another six candidate LyC sources in the GOODS fields at $z \sim 2$ (all with $f_{\rm esc} \gtrsim 13\%$) using *HST*/WFC3 imaging in the F275W and F336W bands from the *Hubble* Deep UV (HDUV) Legacy Survey (GO13872; Oesch et al. 2018). At the redshifts probed by Naidu et al. (2017), the Lyman break lies at ∼2750 Å, such that both ionizing and nonionizing photons fall within the F275W window. To determine the true contribution of LyC photons to the F275W flux then requires somewhat sophisticated and correspondingly uncertain modeling, along with Monte Carlo simulations of UV color and IGM attenuation. At redshifts greater than ∼2.4, however, the F275W filter exclusively probes LyC photons, making the HDUV data a valuable asset for identifying ionizing sources at high redshifts.

In this paper, we combine new and preexisting optical spectroscopy on the GOODS-N field with the deep, high spatial resolution F275W data from the HDUV survey to obtain limits on the contributions of candidate LyC-emitting galaxies at $z \sim 3$, where the HDUV filter set probes only the Lyman continuum, to the overall ionizing emissivity from star-forming galaxies and low-luminosity AGNs. We also present a new UV grism spectroscopic observation from *HST*/WFC3 of a $z \sim 2.6$ FUV-bright quasar.

In Section 2, we describe the data we used to select and characterize possible high-redshift LyC emitters, including UV and X-ray imaging, optical spectra from Keck/DEIMOS, and G280 grism spectroscopy. In Section 3, we describe our search for candidate LyC emitters and discuss the properties of the sources we found, along with potential sources of contamination by foreground galaxies. In Section 4, we estimate the associated contributions (or limits thereof) to the ionizing background at $z \sim 3$ and compare to the flux required to maintain an ionized IGM at this redshift. In Section 5, we summarize our findings and discuss future prospects for the field.

We assume $\Omega_M = 0.3$, $\Omega_\Lambda = 0.7$, and $H_0 = 70$ km s^{-1} Mpc^{-1} throughout this work. All magnitudes are given in the AB system, defined as $m_{\rm AB} = -2.5 \log f_\nu - 48.60$ for flux density, f_ν, in units of erg s^{-1} cm^{-2} Hz^{-1}.

2. Data

2.1. F275W Imaging

The HDUV survey (GO13872; Oesch et al. 2018) is a 132-orbit WFC3 imaging program centered on the GOODS-North and South fields. Designed to capitalize on existing WFC3/UVIS imaging from the CANDELS (Grogin et al. 2011; Koekemoer et al. 2011) and UVUDF (Teplitz et al. 2013; Rafelski et al. 2015) surveys, the HDUV survey imaged both of these fields in the F275W and F336W filters around or within the existing CANDELS and UVUDF footprints. When combined with imaging from each of these surveys, the reduced HDUV images achieve depths of ≈27.5 and 27.9 mag in the F275W and F336W filters, respectively (5σ detection, $0\farcs4$ diameter aperture). Since the Lyman continuum is redshifted into the F275W bandpass at $z > 2.4$, the deep and relatively wide F275W coverage provided by the HDUV survey enables us to search for potential sources of ionizing radiation at high redshift.

2.2. Optical/NIR Spectroscopy

Secure spectroscopic redshifts are required for reliable identification of candidate LyC emitters within our F275W sample. The GOODS-N field is one of the most heavily studied regions of the sky, with a wealth of existing spectroscopic data from DEIMOS on Keck I and LRIS and MOSFIRE on Keck II (e.g., Cohen et al. 2000; Cowie et al. 2004, 2016; Swinbank et al. 2004; Wirth et al. 2004, 2015; Chapman et al. 2005; Reddy et al. 2006; Barger et al. 2008; Trouille et al. 2008; Cooper et al. 2011; Kriek et al. 2015; U et al. 2015). We cross-matched our sample (defined in Section 3.1) to existing Keck spectroscopic catalogs to determine redshifts, then used DEIMOS to target any F275W source in our sample without existing spectroscopic identifications, or to obtain additional spectra of candidate LyC emitters to check for possible contamination by foreground galaxies (see Sections 3.3.1–3.3.6).

For our new DEIMOS observations, we used the 600 line mm^{-1} grating, giving a $d\lambda$ of 3.5 Å and a wavelength coverage of 5300 Å. We centered the spectra at an average wavelength of 7200 Å, but the exact wavelength range for each spectrum depends on the position of the slit in the mask. We broke each ∼1 hr exposure into three subexposures positioned at a central position and two offset positions stepped $1\farcs5$ in each direction along the slit. Our dithering procedure provides extremely high-precision sky subtraction. We reduced the spectra following the procedures described in Cowie et al. (1996).

2.3. UV Grism Spectroscopy

The *HST*/WFC3 grism spectrum from program GO12479 (PI: Hu) was based on 5 dithered observations with the G280 grism. Each observation was 475 s, giving a total exposure time of 2375 s. We also obtained a 120 s imaging exposure with the F2000LP filter to set the zero point for computing the shape of the spectrum and the wavelength calibration. The

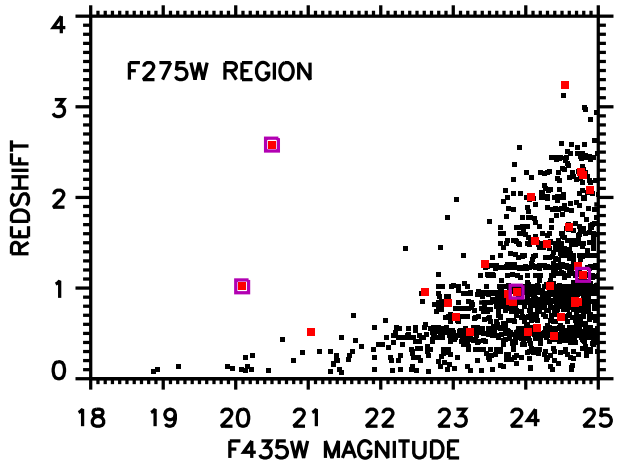

Figure 1. Spectroscopic redshift vs. F435W (B) magnitude for the 68 arcmin^2 area covered by the HDUV GOODS-N F275W image. Sources with no X-ray counterpart are denoted by black squares, while sources with an X-ray detection are denoted by red squares, and those with quasar X-ray luminosities are enclosed in purple open squares. The spectroscopic identifications only start to become significantly incomplete (82% identified) at B magnitudes of 24.5–25.

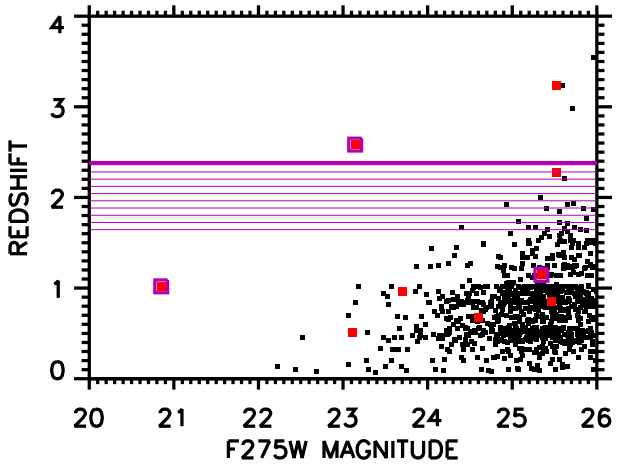

Figure 2. Spectroscopic redshift vs. F275W magnitude for the 68 arcmin^2 area covered by the HDUV GOODS-N F275W image. Sources with no X-ray counterpart are denoted by black squares, while sources with an X-ray detection are denoted by red squares, and those with quasar X-ray luminosities are enclosed in purple open squares. The thick purple line marks the redshift above which the F275W filter is sampling solely below the Lyman continuum break ($z = 2.36$). The purple hatched region shows the redshift range where the break falls within the filter bandpass. The spectroscopic identifications only start to become significantly incomplete (68% identified) at F275W magnitudes of 25.5–26.

G280 grism extends to a short wavelength of 1900 Å with a resolution of 70 at 3000 Å, giving coverage down to a rest wavelength of 530 Å. We measured the flux from the first-order spectrum using the calibrations of the spatial distortion and wavelength relative to the zeroth-order given in Kuntschner et al. (2009). We extracted the spectrum as a function of wavelength with a 6 pixel (0.″24) boxcar centered on the central position of the spectrum. Finally, we flux calibrated the spectrum in units of microjansky, though the absolute calibration is not critical in the present analysis.

2.4. X-Ray Imaging

To identify probable AGNs in our F275W sample, we used X-ray data from the 2 Ms *Chandra X-ray Observatory* exposure of the *Chandra* Deep Field-North (Alexander et al. 2003; Xue et al. 2016). This image reaches a limiting flux of $f_{0.5-2\,\mathrm{keV}} \approx 1.5 \times 10^{-17}$ erg cm^{-2} s^{-1} near the central aim point. We used a 1.″5 search radius to identify X-ray counterparts to sources in our F275W sample; 60 had X-ray counterparts. We computed the rest-frame 2–8 keV luminosities, L_X, of these counterparts from the 0.5–2 keV fluxes with an assumed $\Gamma = 1.8$ and no absorption correction using

$$L_X = 4\pi d_L^2 f_{0.5-2\,\mathrm{keV}} \left(\frac{1+z}{4}\right)^{\Gamma-2} \mathrm{erg\ s^{-1}}. \quad (1)$$

We classify any source with an X-ray luminosity $L_X > 10^{44}$ erg s^{-1} as a quasar (red squares enclosed by a purple open square in Figure 1).

3. Search for $z \sim 3$ Candidate LyC Emitters

3.1. F275W Sample

We started with all $z_{850} < 26$ galaxies from the 140 arcmin^2 GOODS-N observations of Giavalisco et al. (2004) obtained with *HST*'s Advanced Camera for Surveys (ACS). At $z \sim 3$, the ACS F850LP filter probes the rest-frame FUV at ~2300 Å, providing a good selection of likely star-forming galaxies at these redshifts.

We then restricted to the 68 arcmin^2 area where there is F275W coverage with rms errors fainter than 27 mag. There are 5712 sources with $z_{850} < 26$ in this area. In Figure 1, we plot redshift versus F435W (B) magnitude for this area. The spectroscopic identifications are 98% complete to $B = 24.5$, 95% in $B = 24$–24.5, and 82% in $B = 24.5$–25.

We next measured the F275W magnitudes within 1″ diameter apertures at the positions of each $z_{850} < 26$ source using a customized IDL routine and subtracting the background using the median in a 3″–6″ annulus. Magnitude errors were measured from the associated rms noise files. We hereafter consider the 1063 sources with F275W magnitudes brighter than 26 (4σ) as our UV sample.

In Figure 2, we show redshift versus F275W magnitude for this sample. Our spectroscopic identifications are 99% complete to F275W = 25.5, 98% in F275W = 25–25.5 (seven objects missing or unidentified), and 77% complete in F275W = 25.5–26.

Only five sources in Figure 2 lie above the $z \sim 2.4$ threshold (thick purple line) where the F275W flux consists solely of LyC photons (assuming no contamination from foreground sources). One of these sources is an X-ray AGN, and another is an X-ray quasar.

3.2. Color-selected Sample

Alternatively, we can utilize a color selection to search for candidate ionizing sources. In order to have a substantially complete spectroscopic sample, we start with sources with $B < 25$ (see Figure 1). We then use V–$z_{850} < 1$ to select galaxies with relatively flat UV continua (i.e., likely star-forming galaxies) at high redshifts. We plot F275W−F435W versus redshift in Figure 3 for the sources that meet these criteria. We indicate with purple hatching the redshift range

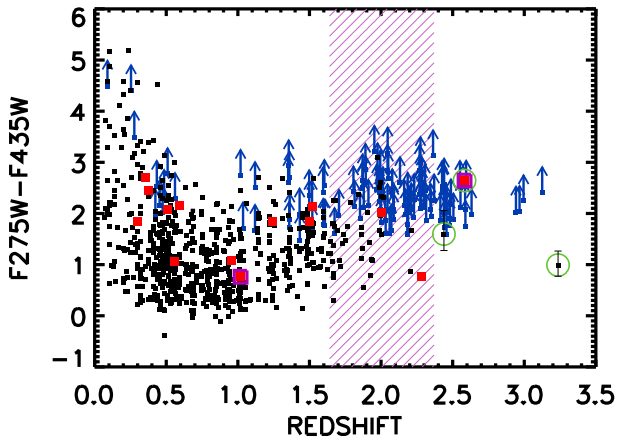

Figure 3. Observed F275W−F435W vs. redshift for $B < 25$ galaxies with flat rest-frame UV continua (i.e., selected using V–$z_{850} < 1$). Sources with no X-ray counterpart are denoted by black squares, while sources with an X-ray detection are denoted by red squares, and those with quasar X-ray luminosities are enclosed in purple open squares. Sources with lower limits on F275W −F435W are plotted at their 2σ values with blue upward pointing arrows. The purple hatched region marks the redshift range where the F275W filter straddles the Lyman break. The three sources enclosed in green open circles have measured F275W−F435W colors at $>2\sigma$ significance and are shown with error bars that reflect the 1σ uncertainties in the F275W magnitudes.

where the F275W filter straddles the Lyman break. The typical color becomes noticeably redder around $z \sim 2$ as the LyC break moves into this window, with most objects at $z \gtrsim 2$ having so little F275W flux that we can measure only lower limits on the color. We find three $z > 2.36$ sources that have measured F275W–F435W colors at the $>2\sigma$ level. We show these with error bars and enclosed in green circles in Figure 3. Two of these color-selected sources also fall into our F275W-selected sample (see Section 3.1) and appear in Figure 2 (one is the X-ray quasar), while the third is detected at the 2.9σ level in F275W.

3.3. Six Candidate LyC Emitters

In Table 1, we list the basic properties of our six candidate LyC emitters, including ID number, decimal coordinates, ground-based spectroscopic and (when available) *HST* grism redshifts, X-ray luminosities, F275W, *B*, and *V* magnitudes, and ionization fraction $f_{\rm ion}$ (see Section 4). We show in Figure 4 both the F275W thumbnail (left) and three-color thumbnail (right; red = F160W, green = F606W, blue = F435W) images of each source. In the following subsections, we briefly discuss for each of the six sources individually our efforts to try and confirm the LyC emission from the $z \sim 3$ sources.

3.3.1. GN-UVC-1

The broad-line quasar GN-UVC-1 at $z = 2.583$ with an F275W magnitude of 23.14 is easily the brightest of our six candidate LyC emitters. The smaller F275W source to its lower right (see Figure 4) is likely a star-forming galaxy at low redshift. GN-UVC-1 is one of two objects in our candidate sample (the other being GN-UVC-3) that was selected both by its F275W flux alone and by its relatively blue F275W–F435W color (≈2.6 mag). As shown in Figure 5, the *HST*/WFC3 G280 grism spectrum of GN-UVC-1 (GO12479, PI: Hu) directly confirms its identification as a high-redshift LyC emitter.

3.3.2. GN-UVC-2

GN-UVC-2 illustrates particularly well the difficulties of trying to confirm LyC emission from high-redshift galaxies. There are two positions in the F275W image (see Figure 4) that show significant UV flux: one coinciding with a somewhat extended star-forming galaxy/possible weak AGN ($L_X \sim 6 \times 10^{42}$ erg s^{-1}) roughly at image center, and one coinciding with a neighboring source about 1″ away. In Figure 6, we show our DEIMOS spectrum with a total exposure time of ∼6 hr. In the individual exposures, we used a 1″ wide slit and slit position angles ranging from 41° to 59°. We visually identify two redshift systems in the spectrum. Absorption features from the extended, central $z = 3.236$ source (Lα, C IV1550, and Al III1670, marked in blue on the spectrum) are clearly present, but so are emission lines ([O II] 3727, Hβ and [O III]4959,5007) from a $z = 0.512$ foreground source (marked in red). We note that at the position angles of the individual spectra, the neighboring source is located just outside the slit. Thus, it is unlikely that it could be the source of the emission lines, since the lines would have to be extraordinarily strong to overflow into the slit at these position angles. Moreover, the emission lines seen in the individual spectra are invariant from exposure to exposure, despite changes in position angle. This suggests that the low-redshift emission lines come from a source superposed more or less directly on top of the $z = 3.236$ galaxy, calling into question the origin of the measured F275W flux.

In Figure 7(a), we show the F275W (blue curve) and F160W (red curve) continuum light profiles as they would appear in a 1″ wide slit at a position angle of 116° that covers both the central and neighboring sources (the relative normalization of the profiles is arbitrary). There is significant UV continuum flux at both positions.

We next obtained an additional 1 hr DEIMOS spectrum (1″ wide slit and 0.″6 seeing) at this position angle. If we examine the [O III] λ5007 light profile from this new spectrum (Figure 7(b)), we see that there is [O III] emission (blue curve) at both positions. The [O III] profile is somewhat smoothed relative to the *HST* continuum data in Figure 7(a) due to the seeing. However, at the positions of both the central and neighboring sources, it is significantly brighter than the continuum measured both 300 Å redward and blueward of the line center (red curves). This confirms that the neighboring source is also at $z \sim 0.5$.

We consequently interpret the low-redshift emission lines as coming from a $z \sim 0.5$ galaxy with two spatially separated star-forming components (i.e., similar to the chain galaxies of Cowie et al. (1995) and references therein), one of which lies directly along the line of sight to the high-redshift Lyman-break galaxy (LBG). Thus, the bulk of the measured F275W flux probably comes from the low-redshift galaxy, meaning GN-UVC-2 should not be used when constraining the ionizing background at $z \sim 3$. We exclude it from our analysis in Section 4.

3.3.3. GN-UVC-3

We show in Figure 8 our DEIMOS spectrum of GN-UVC-3. As with GN-UVC-2, spectral features from a $z = 3.239$ source (Lyα emission and C IV1550 absorption marked in blue) and from a foreground $z = 0.56$ source ([O II]3727, Hβ, and [O III] 4959,5007 emission marked in red) are visually identified. The

Table 1
Summary of Six Candidate LyC Emitters

ID[a]	R.A.	Decl.	z_{spec}[b]	z_{grism}[c]	L_X	F275W	$F435W_{AB}$	$F606W_{AB}$	f_{ion}[d]
GN-UVC-1 (1, 2)	189.095581	+62.257492	2.583 (I)	2.597	3.44×10^{44}	23.14	20.50	20.49	0.087
GN-UVC-2 (1)	189.179535	+62.185806	3.236 (I)	3.299	5.66×10^{42}	25.53	24.54	23.40	⋯
GN-UVC-3 (1, 2)	189.275543	+62.250462	3.239 (I, II)	⋯	⋯	25.60	25.21	24.46	⋯
GN-UVC-4 (1)	189.148758	+62.271030	2.984 (I, II)	⋯	⋯	25.71	25.05	24.58	⋯
GN-UVC-5 (1)	189.296936	+62.270989	3.546 (I, III)	⋯	⋯	25.96	25.77	25.44	⋯
GN-UVC-6 (2)	189.201889	+62.266682	2.439 (II)	⋯	⋯	26.53	24.93	24.74	0.193

Notes.
[a] Parenthetical numbers indicate if a candidate was selected by (1) its F275W magnitude, (2) its F275W–F435W color, or both.
[b] Spectroscopic redshifts from (I) this work; (II) Reddy et al. (2006); and (III) U et al. (2015).
[c] Determined from G280 grism data from *HST*/WFC3 (GO12479, PI: Hu) for GN-UVC-1, and from G141 grism data from the 3D-*HST* survey (Momcheva et al. 2016) for GN-UVC-2.
[d] Ratio of F275W flux to F606W flux (rest-frame ∼675–1500 Å; see Section 4).

high-redshift system was previously identified by Reddy et al. (2006). The low-redshift interloper is almost certainly the source of the F275W flux. Thus, we also exclude GN-UVC-3 from our analysis in Section 4.

3.3.4. GN-UVC-4

GN-UVC-4 is peculiar, because its *BVH* thumbnail in Figure 4 shows at least two differently colored components (a redder source at image center and an elongated, clumpy, blue source extending northward). However, the UV emission corresponds only to the central redder source. Our DEIMOS spectrum confirms the source as a projection of two emission line galaxies at very different redshifts (see Figure 9). The high-redshift identification at $z = 2.984$ is based on Lyα and C IV1550 emission and confirms the redshift obtained by Reddy et al. (2006). The low-redshift identification at $z = 0.760$ is based on [O II]3727, Hβ, and [O III]4959,5007 emission. We conclude that the UV emission probably comes from the low-redshift galaxy. Thus, we exclude GN-UVC-4 from our analysis in Section 4.

3.3.5. GN-UVC-5

The F275W detection of GN-UVC-5 is quite surprising, because by $z = 3.546$, the F275W bandpass probes rest-frame wavelengths well below the LyC break (at ∼590 Å), where we expect virtually no transmission of ionizing radiation from the galaxy due to attenuation by the IGM (e.g., Inoue et al. 2014). U et al. (2015) label this object as having a very secure redshift identification (quality code "A"), while photometric redshift estimates given in the 3D-*HST* catalog (Momcheva et al. 2016) put GN-UVC-5 (their GN-26359) at $z_{phot} = 0.74$. These conflicting redshift estimates, together with the apparently singular nature in F275W of GN-UVC-5 (see Figure 4), suggest that this source may be yet another chance projection of two galaxies at vastly different redshifts. Indeed, our DEIMOS spectrum shows weak Lyα emission and C IV1550 in absorption (see Figure 10), confirming the redshift of U et al. (2015), while also showing [O II]3727, Hβ, and [O III] 4959,5007 emission from a low-redshift galaxy at $z = 0.789$. Since the UV emission probably comes from the low-redshift galaxy, we exclude GN-UVC-5 from our analysis in Section 4.

3.3.6. GN-UVC-6

Of our six candidate LyC emitters, this is the sole object selected only based on its relatively blue F275W–F435W color (≈1.6 mag, bluer even than the bright quasar GN-UVC-1), though we note that it is detected at the 2.9σ level in F275W. We find a possible far-infrared counterpart to this source in the GOODS-*Herschel* catalog of Elbaz et al. (2011; separation $<0\farcs5$). This may indicate the presence of an AGN, though with only one detection from *Herschel* (in the PACS 160 μm band) and negligible X-ray flux, this is somewhat tentative. The complicated morphology and multiple *BVH* colors seen in GN-UVC-6's three-color thumbnail (see Figure 4) suggests that there may be superposed sources that could lie at different redshifts. However, the photometric redshift of $z = 2.38$ from Rafferty et al. (2011) is in good agreement with the spectroscopic redshift of $z = 2.439$ from Reddy et al. (2006), which argues against contamination from foreground objects. We recently obtained a DEIMOS spectrum of this source and confirm that there are no features in the 4500–10000 Å range that would indicate the presence of a superposed foreground object. We conclude that GN-UVC-6 remains a good candidate LyC emitter and can be used to obtain limits on the contribution of galaxies to the ionizing background at $z \sim 3$.

4. Contributions to the Ionizing Flux

Determining the absolute escape fraction for each of our candidate LyC emitters is challenging, if not impossible, without knowledge of each source's intrinsic spectral energy distribution (SED) and degree of reddening. Instead, we compute the ionization fraction from $f_{ion} = f_{LyC}/f_{1500}$; that is, the ratio of the flux at the rest-frame LyC wavelength (∼675 Å at $z = 3$) to the flux at rest-frame 1500 Å, ignoring the small differential *K*-correction as a function of redshift. We use the F606W flux as a rough estimate of the rest-frame 1500 Å flux, assuming a flat f_ν SED. We note that this approximation is most accurate for sources very near $z = 3$. We give our measured ionization fractions in the last column of Table 1 for the two sources that do not have clear spectroscopic evidence for contamination by foreground galaxies.

4.1. Quasar UV Emissivity

GN-UVC-1 is brighter than any other candidate in our sample by approximately two magnitudes. Since it is also the only quasar, we consider its contribution to the ionizing background separately

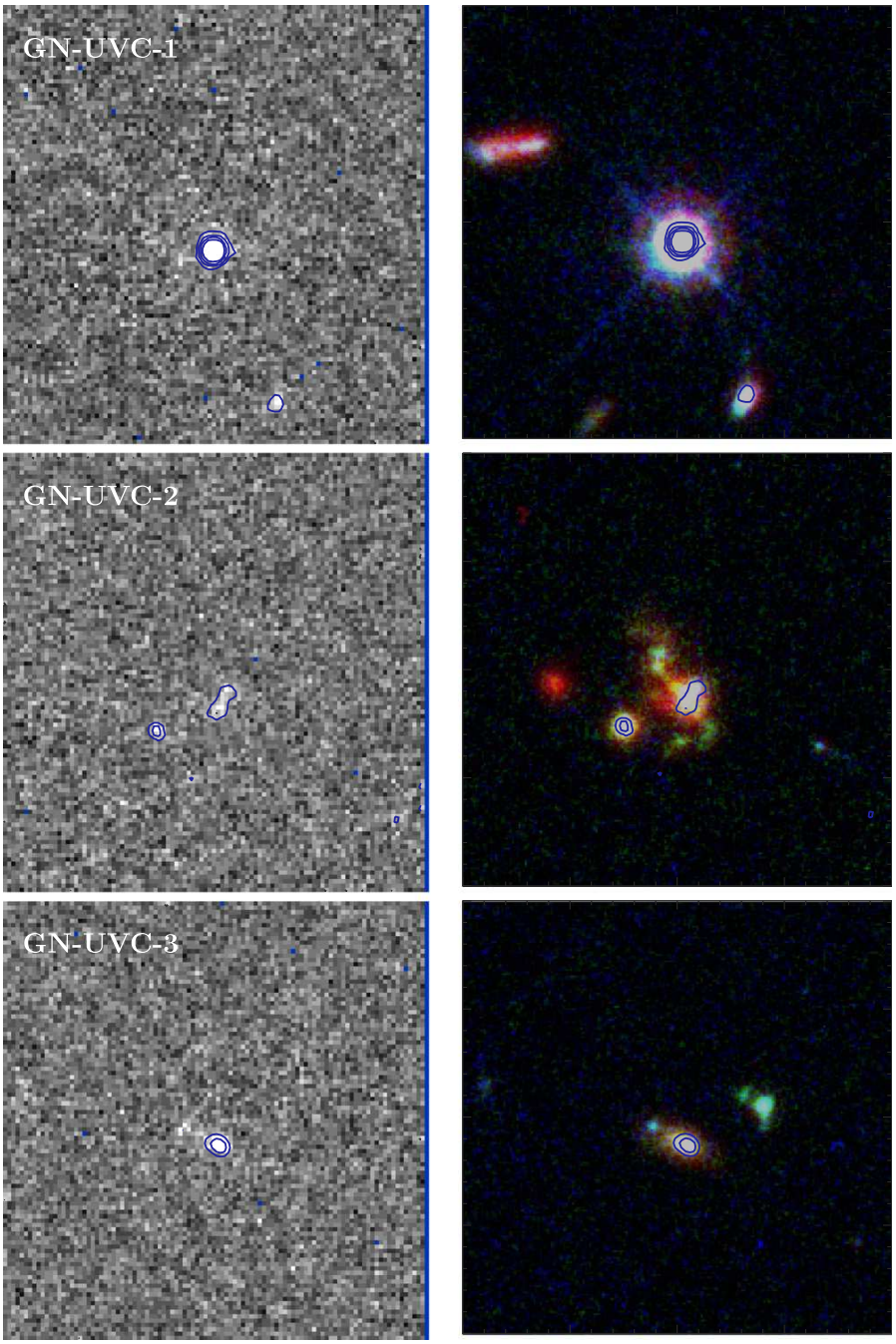

Figure 4. F275W thumbnails (left) and three-color images (red = F160W, green = F606W, and blue = F435W) of our six candidate LyC emitters. Blue contours show F275W emission for sources detected at or above the 4σ level in the HDUV F275W imaging. (Note that GN-UVC-6 is detected at the 2.9σ level in F275W and was selected based on its relatively blue F275W–F435W color; see Section 3.) Images are $6''$ on a side. North is up and east is to the left. The sources appear slightly below center in y to allow for the labels at the top.

from our other candidates. We measured its flux density at 912 Å directly from its UV grism spectrum after renormalizing the spectrum to match the total flux detected in the F275W imaging data. We then converted this to an ionizing volume emissivity, ϵ_{912}, defined as the luminosity density per unit frequency divided by the comoving volume over the redshift range of $z = 2.439$–3.546 (the lowest and highest redshifts of our candidates). We hereafter quote measurements and uncertainties of ϵ_{912} in units of 10^{24} erg s^{-1} Hz^{-1} Mpc^{-3}. For the single source in our "quasar sample," the Poisson noise dominates; from Gehrels (1986), the 68% confidence range for one object is 0.173–3.300. We find a quasar UV emissivity, $\epsilon_{912,q}$, of $8.3^{27}_{1.4}$.

4.2. Nonquasar UV Emissivity

With four of five nonquasar candidates showing clear contamination from foreground objects, our "star-forming

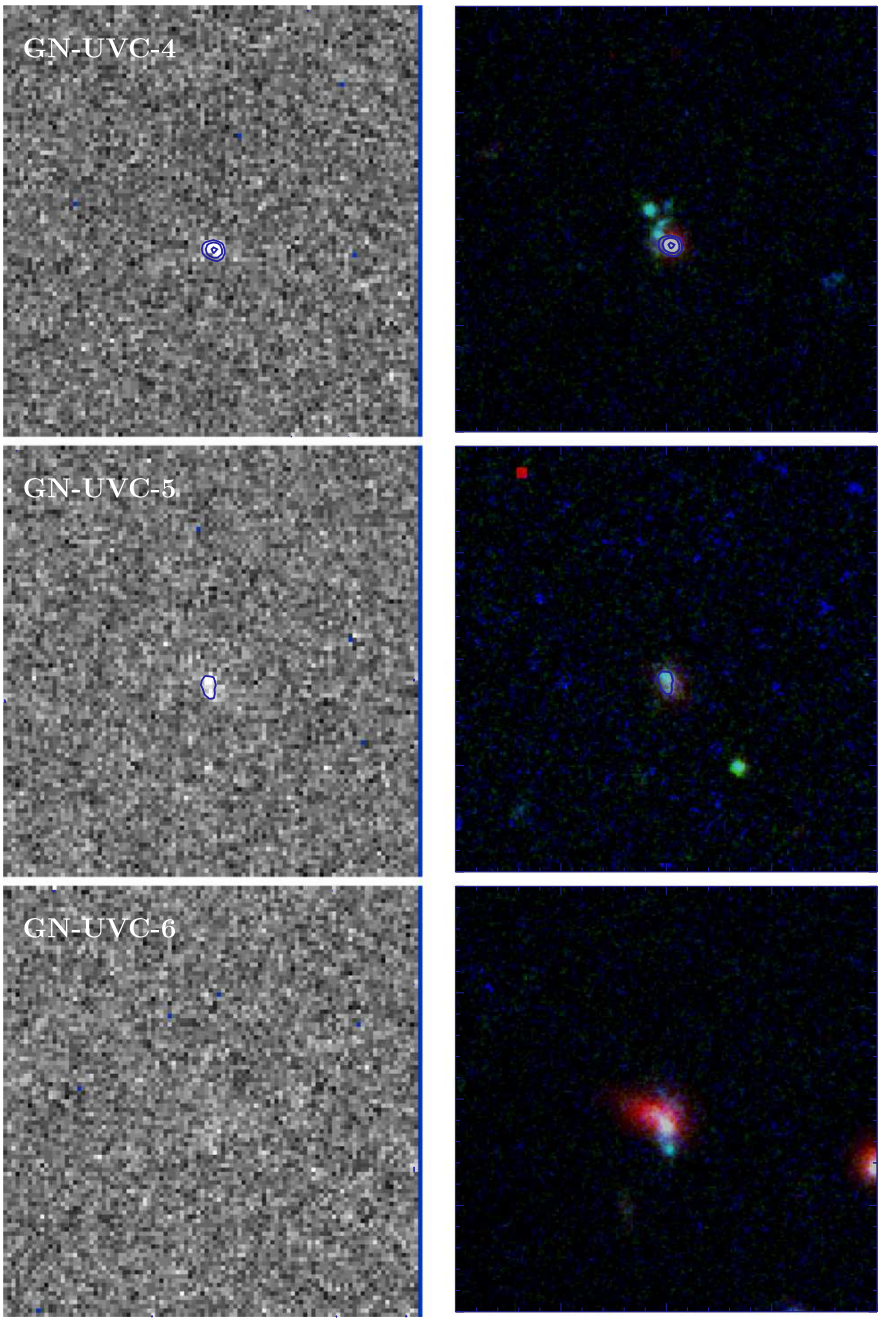

Figure 4. (Continued.)

galaxy" sample considered here consists of GN-UVC-6 only. We estimated an ionizing emissivity $\epsilon_{912,g}$ for this likely star-forming galaxy/possible low-luminosity AGN by assuming that GN-UVC-6's F275W flux is entirely at the filter's effective wavelength of ∼2704 Å, or rest-frame ∼786 Å. To allow for a simpler and more direct comparison with literature results, which mostly consider the ionizing volume emissivity at or near the LyC edge, we scaled the measured flux density to that at 912 Å following the results of Lusso et al. (2015). They used a sample of 53 quasars at $z \sim 2.4$ to construct a stacked UV spectrum between 600 and 2500 Å (rest frame), correcting for both intergalactic Lyman forest and Lyman continuum absorption, and found a $\lambda < 912$ Å continuum slope of $\alpha_\nu = -1.70$. We used this power-law slope to do our scaling. We find that GN-UVC-6 contributes $\epsilon_{912,g} = 0.22^{0.72}_{0.04}$ to the ionizing background at $z \sim 3$, where the total error is again dominated by the Poisson noise (in the 68% confidence range).

4.3. Comparisons with the Literature

In Figure 11, we put our measurements in the context of other $z \sim 3$ measurements from the literature. The level of

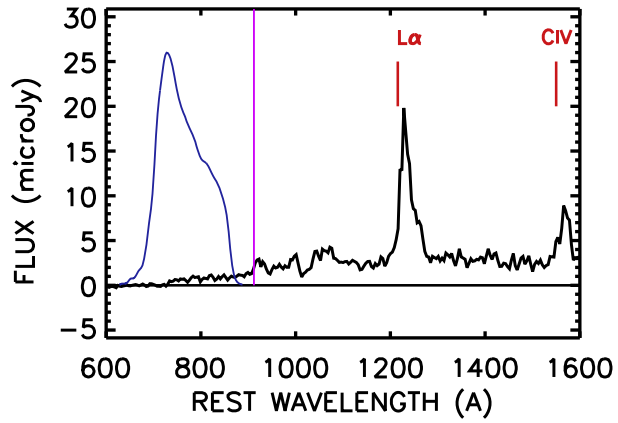

Figure 5. G280 grism spectrum from *HST*/WFC3 for GN-UVC-1. The blue curve shows the relative response of the F275W filter shifted into the rest frame of GN-UVC-1, and the pink vertical line marks the LyC edge.

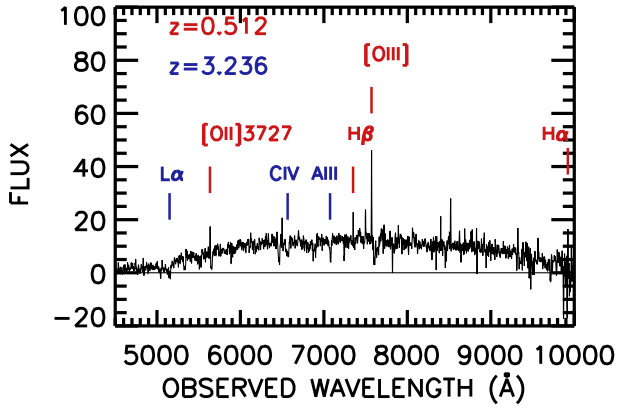

Figure 6. Our DEIMOS spectrum of GN-UVC-2. In addition to absorption features from a $z = 3.236$ galaxy (marked in blue), emission lines from a foreground galaxy at $z = 0.512$ (marked in red) are clearly present.

ionizing volume emissivity that we estimated from our single quasar (gold star) is a factor of $\sim$38 larger than our $\epsilon_{912,g}$ (bronze circle). Though our small sample size makes quantitative comparisons difficult, our $\epsilon_{912,q}$ is consistent, within the very large uncertainties, with the contribution measured by CBT09 from their much larger sample of broad-line AGNs (their Equation (1); red curve and points in Figure 11). It is also roughly consistent with quasar ionizing emissivity results from Meiksin (2005; gray curve) and Haardt & Madau (2012; purple curve).

Becker & Bolton (2013) used Lyα forest observations to infer the total ionizing background from $2 < z < 5$. They obtained a nominal $\epsilon_{912} = 8.15$ at $z = 3.2$, again a factor of $\sim$38 larger than our upper-limit estimate of $\epsilon_{912,g}$ but consistent with our measured contribution from quasars. This suggests that quasars alone contribute virtually all of the metagalactic ionizing background at these redshifts. However, we caution that GN-UVC-1-like quasars are likely quite rare. The presence of such a LyC-luminous source in the relatively small comoving volume studied here is probably serendipitous, and a wider survey area (such as that used in CBT09) is needed to mitigate the effects of cosmic variance.

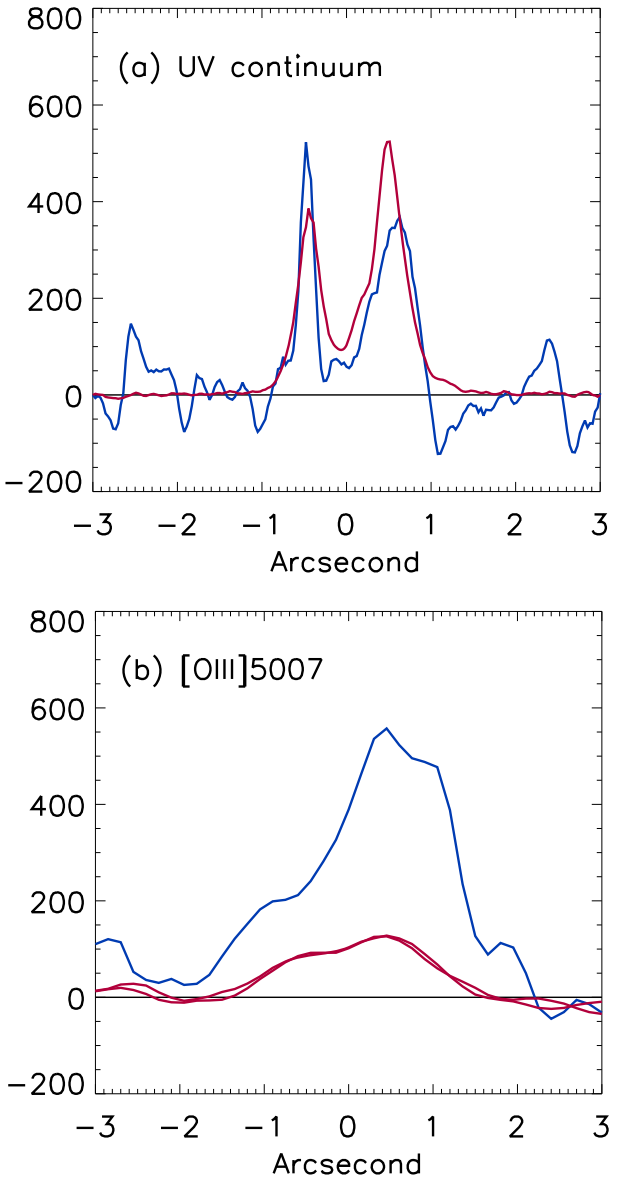

Figure 7. (a) The F275W (blue curve) and F160W (red curve) light profiles as they would appear in a 1″ wide slit at a position angle of 116° that crosses both the LBG and the neighboring source in the GN-UVC-2 image (upper-right thumbnail in Figure 4). The relative normalization of the two profiles in this panel is arbitrary. (b) The light profile of the $z = 0.512$ [O III] λ5007 Å line (blue curve) and the continuum measured both 300 Å redward and blueward of the line (red curves) as seen in a 1 hr Keck/DEIMOS spectrum taken at a position angle of 116°. The 0.″6 seeing smooths the profile considerably relative to the *HST* continuum data, but the [O III] profile lies above the continuum throughout the profile and is clearly present at the positions of both the LBG and the neighboring source.

Meanwhile, for galaxies and/or low-luminosity AGNs like GN-UVC-6 to contribute significantly to the UV background, numerous fainter contributions would be required. We note, for example, that even with the high rate of contamination by foreground galaxies, Figure 2 only starts to become significantly populated at $z \gtrsim 2.4$ for apparent magnitudes approaching our cutoff of F275W = 26.

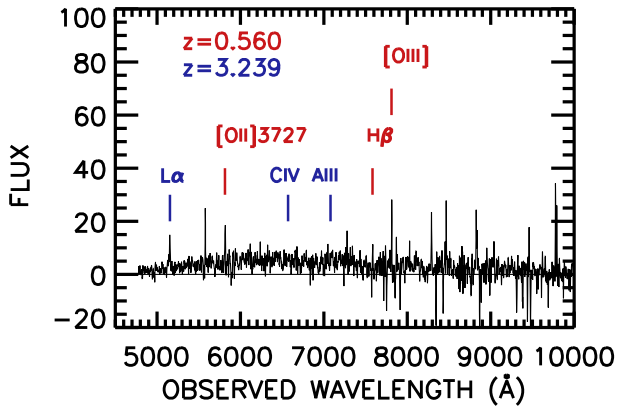

Figure 8. Our DEIMOS spectrum of GN-UVC-3, which shows features from sources at $z = 3.239$ (blue) and $z = 0.56$ (red).

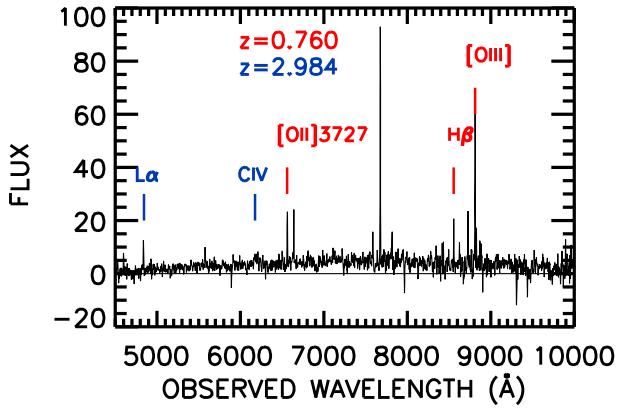

Figure 9. Our DEIMOS spectrum of GN-UVC-4, which shows features from sources at $z = 2.984$ (blue) and $z = 0.76$ (red).

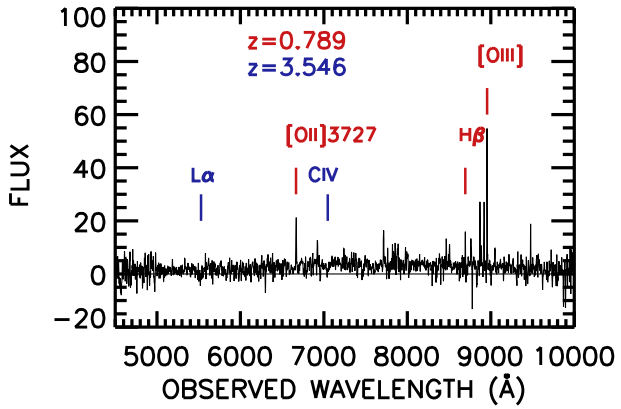

Figure 10. Our DEIMOS spectrum of GN-UVC-5, which shows features from sources at $z = 3.546$ (blue) and $z = 0.789$ (red).

We may also think about the limits of our sample selection in terms of the UV continuum absolute magnitudes $M_{\rm UV}$, usually measured at 1500 or 1600 Å when deriving rest-frame UV luminosity functions (LFs) at various redshifts. Again using the observed F606W magnitudes of our candidate sources as an estimate of the rest-frame 1500 Å flux, we find that our $z \sim 3$ candidate LyC emitters probe as faint as $M_{\rm UV} \approx -22.3$. This is $\sim$1.5 mag brighter than the characteristic luminosities of the $z \sim 7$ rest-frame UV LFs derived in, e.g., Bouwens et al. (2015b; $M^*_{1600} = -20.87$) or Livermore et al. (2017; $M^*_{1500} = -20.80$). If our candidate LyC sources are taken to be analogs to the high-redshift galaxies that are responsible for reionization, these sources would thus still lie firmly on the bright end of the $z \sim 7$ UV LF. Furthermore, even though the very deep *HST* imaging used to construct these high-redshift UV LFs have detection limits as faint as $M_{\rm UV} \sim -14.5$, even this is unable to detect the ultra-faint galaxies that appear to be required to complete hydrogen reionization by $z \sim 6$ (e.g., Finkelstein et al. 2015; Livermore et al. 2017). A more accurate census of $z \sim 3$ analogs to the very-high-redshift sources that drove reionization will require deeper F275W imaging and corresponding spectroscopic follow-up, though at such faint magnitudes, redshift identifications are quite difficult.

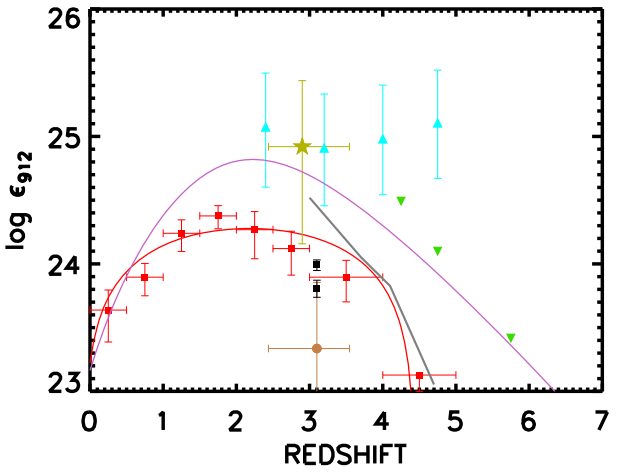

Figure 11. Ionizing volume emissivity at $z = 3$ estimated from the quasar GN-UVC-1 (gold star) and compared to literature results for quasar/AGN contributions to the ionizing background at similar redshifts. Red, green, and black symbols show data from CBT09, Parsa et al. (2018), and Micheva et al. (2016), respectively, and the red, purple, and gray curves are from CBT09, Haardt & Madau (2012), and Meiksin (2005), respectively. The bronze circle shows the ionizing emissivity from star-forming galaxies and low-luminosity AGNs identified in this work (e.g., GN-UVC-6). Horizontal error bars on our data points reflect the range of redshifts in our candidate sample; the symbols have been splayed around the mean redshift of 3 for clarity. Cyan triangles show the observed ionizing emissivity from Becker & Bolton (2013).

5. Summary

We have presented a search for candidate LyC emitters at $z \sim 3$ in the GOODS-North field using deep *HST*/WFC3 F275W imaging data and highly complete Keck/DEIMOS spectroscopic follow-up. We found five candidate ionizing sources brighter than F275W = 26, plus one additional source with blue F275W−F435W colors selected from a $B < 25$ sample with colors $V - z_{850} < 1$. One candidate (GN-UVC-1) is a $z \sim 2.5$ quasar that, at F275W $\sim$23.1, is exceptionally bright at rest-frame wavelengths blueward of the Lyman limit. UV grism spectroscopy from *HST*/WFC3 confirms the presence of significant LyC flux. Four candidates each appear to be contaminated by a foreground $z \sim 0.5$–0.7 galaxy based on deep optical spectroscopy.

The contribution of the quasar GN-UVC-1 to the ionizing background at $z \sim 3$ totally dominates over the contributions from candidate LyC-emitting galaxies and faint AGNs (that is, GN-UVC-6, the sole nonquasar candidate source with no

obvious contamination). Modulo potential currently undetected contamination by lower redshift sources and the effects of cosmic variance, together they could account for the total ionizing background at $z \sim 3$. However, for galaxies and low-luminosity AGNs alone to account for all (or even a non-negligible portion of) the total ionizing background at $z \sim 3$, significant additional contributions from fainter sources would be needed. This will require deeper and wider area surveys to probe.

We gratefully acknowledge support from NASA grant NNX14AJ66G and NSF grant AST-1715145, the Trustees of the William F. Vilas Estate, and the University of Wisconsin-Madison Office of the Vice Chancellor for Research and Graduate Education with funding from the Wisconsin Alumni Research Foundation (A.J.B.). Support for program number GO12479 was provided by NASA through a grant from the Space Telescope Science Institute, which is operated by the Association of Universities for Research in Astronomy, Inc., under NASA. Based in part on data obtained at the W. M. Keck Observatory, which is operated as a scientific partnership among the California Institute of Technology, the University of California, and NASA and was made possible by the generous financial support of the W. M. Keck Foundation. The authors wish to recognize and acknowledge the very significant cultural role and reverence that the summit of Maunakea has always had within the indigenous Hawaiian community. We are most fortunate to have the opportunity to conduct observations from this mountain.

ORCID iDs

L. H. Jones https://orcid.org/0000-0002-1706-7370
A. J. Barger https://orcid.org/0000-0002-3306-1606
L. L. Cowie https://orcid.org/0000-0002-6319-1575
P. Oesch https://orcid.org/0000-0001-5851-6649
R. P. Naidu https://orcid.org/0000-0003-3997-5705

References

Alexander, D. M., Bauer, F. E., Brandt, W. N., et al. 2003, AJ, 126, 539
Barger, A. J., Cowie, L. L., Capak, P., et al. 2003, ApJL, 584, L61
Barger, A. J., Cowie, L. L., & Wang, W.-H. 2008, ApJ, 689, 687
Becker, G. D., & Bolton, J. S. 2013, MNRAS, 436, 1023
Bergvall, N., Leitet, E., Zackrisson, E., & Marquart, T. 2013, A&A, 554, A38
Bolton, J. S., & Haehnelt, M. G. 2007, MNRAS, 382, 325
Bolton, J. S., Haehnelt, M. G., Viel, M., & Springel, V. 2005, MNRAS, 357, 1178
Borthakur, S., Heckman, T. M., Leitherer, C., & Overzier, R. A. 2014, Sci, 346, 216
Bouwens, R. J., Illingworth, G. D., Blakeslee, J. P., & Franx, M. 2006, ApJ, 653, 53
Bouwens, R. J., Illingworth, G. D., Oesch, P. A., et al. 2012, ApJL, 752, L5
Bouwens, R. J., Illingworth, G. D., Oesch, P. A., et al. 2015a, ApJ, 811, 140
Bouwens, R. J., Illingworth, G. D., Oesch, P. A., et al. 2015b, ApJ, 803, 34
Chapman, S. C., Blain, A. W., Smail, I., & Ivison, R. J. 2005, ApJ, 622, 772
Cohen, J. G., Hogg, D. W., Blandford, R., et al. 2000, ApJ, 538, 29
Cooper, M. C., Aird, J. A., Coil, A. L., et al. 2011, ApJS, 193, 14
Cowie, L. L., Barger, A. J., & Hu, E. M. 2010, ApJ, 711, 928
Cowie, L. L., Barger, A. J., Hu, E. M., Capak, P., & Songaila, A. 2004, AJ, 127, 3137
Cowie, L. L., Barger, A. J., & Songaila, A. 2016, ApJ, 817, 57
Cowie, L. L., Barger, A. J., & Trouille, L. 2009, ApJ, 692, 1476
Cowie, L. L., Hu, E. M., & Songaila, A. 1995, AJ, 110, 1576
Cowie, L. L., Songaila, A., Hu, E. M., & Cohen, J. G. 1996, AJ, 112, 839
Cristiani, S., Serrano, L. M., Fontanot, F., Vanzella, E., & Monaco, P. 2016, MNRAS, 462, 2478
de Barros, S., Vanzella, E., Amorín, R., et al. 2016, A&A, 585, 51
Elbaz, D., Dickinson, M., Hwang, H. S., et al. 2011, A&A, 533, 119
Faisst, A. L. 2016, ApJ, 829, 99
Faucher-Giguère, C.-A., Lidz, A., Hernquist, L., & Zaldarriaga, M. 2008, ApJ, 688, 85
Feng, Y., Di-Matteo, T., Croft, R. A., et al. 2016, MNRAS, 455, 2778
Fernandez-Soto, A., Lanzetta, K. M., & Chen, H.-W. 2003, MNRAS, 342, 1215
Finkelstein, S. L., Papovich, C., Ryan, R. E., et al. 2015, ApJ, 758, 93
Fontanot, F., Cristiani, S., Monaco, P., et al. 2007, A&A, 461, 39
Fontanot, F., Cristiani, S., Pfrommer, C., Cupani, G., & Vanzella, E. 2014, MNRAS, 438, 2097
Fontanot, F., Cristiani, S., & Vanzella, E. 2012, MNRAS, 425, 1413
Gehrels, N. 1986, ApJ, 303, 336
Georgakakis, A., Aird, J., Buchner, J., et al. 2015, MNRAS, 453, 1946
Giallongo, E., Grazian, A., Fiore, F., et al. 2015, A&A, 578, A83
Giavalisco, M., Ferguson, H. C., Koekemoer, A. M., et al. 2004, ApJL, 600, L93
Grazian, A., Giallongo, E., Gerbasi, R., et al. 2016, A&A, 585, A48
Grazian, A., Giallongo, E., Paris, D., et al. 2017, A&A, 602, A18
Grimes, J. P., Heckman, T., Aloisi, A., et al. 2009, ApJS, 181, 272
Grogin, N. A., Kocevski, D. D., Faber, S. M., et al. 2011, ApJS, 197, 35
Guaita, L., Pentericci, L., Grazian, A., et al. 2016, A&A, 587, A133
Haardt, F., & Madau, P. 2012, ApJ, 746, 125
Inoue, A. K., Shimizu, I., Iwata, I., & Tanaka, M. 2014, MNRAS, 442, 1805
Izotov, Y. I., Orlitová, I., Schaerer, D., et al. 2016a, Natur, 529, 178
Izotov, Y. I., Schaerer, D., Thuan, T. X., et al. 2016b, MNRAS, 461, 3683
Izotov, Y. I., Worseck, G., Schaerer, D., et al. 2018, MNRAS, 478, 4851
Japelj, J., Vanzella, E., Fontanot, F., et al. 2017, MNRAS, 468, 389
Khaire, V., Srianand, R., Choudhury, T. R., & Gaikwad, P. 2016, MNRAS, 457, 4051
Kimm, T., Katz, H., Haehnelt, M. G., et al. 2017, MNRAS, 466, 4826
Koekemoer, A. M., Faber, S. M., Ferguson, H. C., et al. 2011, ApJS, 197, 36
Kriek, M., Shapley, A. E., Reddy, N. A., et al. 2015, ApJS, 218, 15
Kuntschner, H., Bushouse, H., Kummel, M., & Walsh, J. R. 2009, ST-ECF Instrument Science Rep. WFC3 2009-01
Leitet, E., Bergvall, N., Hayes, M., et al. 2013, A&A, 553, A106
Leitherer, C., Ferguson, H. C., Heckman, T. M., & Lowenthal, J. D. 1995, ApJ, 454, 19L
Leitherer, C., Hernandez, S., Lee, J. C., & Oey, M. S. 2016, ApJ, 823, 64L
Livermore, R. C., Finkelstein, S. L., & Lotz, J. M. 2017, ApJ, 835, 113
Lusso, E., Worseck, G., Hennawi, J. F., et al. 2015, MNRAS, 449, 4204
Ma, X., Kasen, D., Hopkins, P. F., et al. 2015, MNRAS, 453, 960
Madau, P. 1995, ApJ, 441, 18
Madau, P., & Haardt, F. 2015, ApJL, 813, L8
Marchi, F., Pentericci, L., Guaita, L., et al. 2018, A&A, 614, 11
Matthee, J., Sobral, D., Best, P., et al. 2017, MNRAS, 465, 3637
Meiksin, A. 2005, MNRAS, 356, 596
Micheva, G., Iwata, I., & Inoue, A. K. 2016, MNRAS, 465, 302
Mitra, S., Ferrara, A., & Choudhury, T. R. 2013, MNRAS, 428, L1
Momcheva, I. G., Brammer, G. B., van Dokkum, P. G., et al. 2016, ApJS, 225, 27
Mostardi, R. E., Shapley, A. E., Steidel, C. C., et al. 2015, ApJ, 810, 107
Naidu, R. P., Forrest, B., Oesch, P. A., et al. 2018, MNRAS, 478, 791
Naidu, R. P., Oesch, P. A., Reddy, N., et al. 2017, ApJ, 847, 12
Oesch, P. A., Montes, M., Reddy, N., et al. 2018, ApJS, 237, 12
Ouchi, M., Mobasher, B., Shimasaku, K., et al. 2009, ApJ, 706, 1136
Parsa, S., Dunlop, J. S., & McLure, R. J. 2018, MNRAS, 474, 2904
Price, L. C., Trac, H., & Cen, R. 2016, arXiv:1605.03970
Puchwein, E., Haardt, F., Haehnelt, M. G., & Madau, P. 2018, MNRAS, submitted (arXiv:1801.04931)
Rafelski, M., Teplitz, H. I., Gardner, J. P., et al. 2015, AJ, 150, 31
Rafferty, D. A., Brandt, W. N., Alexander, D. M., et al. 2011, ApJ, 742, 3
Reddy, N. A., Steidel, C. C., Erb, D. K., Shapley, A. E., & Pettini, M. 2006, ApJ, 653, 1004
Riccoti, M., & Shull, J. M. 2000, ApJ, 542, 548
Robertson, B. E., Ellis, R. S., Dunlop, J. S., McLure, R. J., & Stark, D. P. 2010, Natur, 468, 49
Robertson, B. E., Ellis, R. S., Furlanetto, S. R., & Dunlop, J. S. 2015, ApJL, 802, L19
Rutkowski, M. J., Scarlata, C., Haardt, F., et al. 2016, ApJ, 819, 81
Rutkowski, M. J., Scarlata, C., Henry, A., et al. 2017, ApJL, 841, 27
Shapley, A. E., Steidel, C. C., Strom, A. L., et al. 2016, ApJL, 826, L24
Siana, B., Shapley, A. E., Kulas, K. R., et al. 2015, ApJ, 804, 17
Siana, B., Teplitz, H. I., Ferguson, H. C., et al. 2010, ApJ, 723, 241
Smith, B. M., Windhorst, R. A., Jansen, R. A., et al. 2018, ApJ, 853, 191
Songaila, A. 2004, AJ, 127, 2598

Steidel, C. C., Bogosavlevic, M., Shapley, A. E., et al. 2018, ApJ, submitted (arXiv:1805.06071)
Steidel., C. C., Pettini, M., & Adelberger, K. L. 2001, ApJ, 546, 665
Swinbank, A. M., Smail, I., Chapman, S. C., et al. 2004, ApJ, 617, 64
Teplitz, H. I., Rafelski, M., Kurczynski, P., et al. 2013, AJ, 146, 159
Trouille, L., Barger, A. J., Cowie, L. L., Yang, Y., & Mushotzky, R. F. 2008, ApJ, 179, 1
U, V., Hemmati, S., Darvish, B., et al. 2015, ApJ, 815, 57
Vanzella, E., de Barros, S., Castellano, M., et al. 2015, A&A, 576, A116
Vanzella, E., de Barros, S., Vasei, K., et al. 2016, ApJ, 825, 41
Vanzella, E., Giavalisco, M., Inoue, A. K., et al. 2010a, ApJ, 725, 1011
Vanzella, E., Guo, Y., Giavalisco, M., et al. 2012, ApJ, 751, 70
Vanzella, E., Nonino, M., Cristiani, S., et al. 2012, MNRAS, 424, 54
Vanzella, E., Siana, B., Cristiani, S., & Nonino, M. 2010b, MNRAS, 404 1672
Wirth, G. D., Trump, J. R., Barro, G., et al. 2015, AJ, 150, 153
Wirth, G. D., Willmer, C. N. A., Amico, P., et al. 2004, AJ, 127, 3121
Xue, Y. Q., Luo, B., Brandt, W. N., et al. 2016, ApJS, 224, 15